Remote Sensing of Environment 234 (2019) 111451

Contents lists available at ScienceDirect

Remote Sensing of Environment

journal homepage: www.elsevier.com/locate/rse

Can vegetation optical depth reflect changes in leaf water potential during soil moisture dry-down events?

Yao Zhang[a,b,c,*], Sha Zhou[b], Pierre Gentine[b], Xiangming Xiao[a]

[a] Department of Microbiology and Plant Biology, Center for Spatial Analysis, University of Oklahoma, Norman, OK, USA
[b] Department of Earth and Environmental Engineering, Columbia University, New York, NY, USA
[c] Climate and Ecosystem Division, Lawrence Berkeley National Laboratory, Berkeley, CA, USA

ARTICLE INFO

Keywords:
Iso/anisohydricity
Biomass
Soil water potential
Mesonet
AMSR-E
Water use strategy

ABSTRACT

Plant water use strategy is one of the key factors to predict drought impact on vegetation and land-atmosphere fluxes. Vegetation optical depth (VOD) based on microwave radiative transfer inversion has recently been used to assess plant water use strategy. However, VOD is sensitive to both total aboveground biomass (AGB) and leaf water content, with only the latter being a proxy of leaf water potential whose diurnal variation can be used to characterize vegetation iso/anisohydricity. In this study, by using a network of soil water measurements (used as a proxy for predawn leaf water potential), satellite retrieved normalized difference vegetation index (NDVI, as a proxy for AGB), and two satellite VOD products from the Advanced Microwave Scanning Radiometer-Earth Observing System (AMSR-E) sensor, we compare three linear models and one machine learning model to investigate to what extent can VOD be used to represent leaf water potential changes during soil moisture dry-down periods. Linear models with both NDVI and leaf water potential, on average, can explain 33% and 51% of VOD variations of each product respectively. Models using only NDVI explain 27% and 46% of the VOD variance, compared to less than 10% by models using leaf water potential only. With the NDVI and leaf water potential (full) model, leaf water potential contributes around 17% of the VOD variance, which is smaller than NDVI (33%). The machine learning model has overall better performance than the linear models, and also highlight the dominant contribution of AGB to VOD signals. After the AGB contribution to VOD is eliminated by normalizing daytime VOD with nighttime VOD, the residuals carry the information of diurnal variations of leaf water potential and calculations from both VOD datasets are consistent with each other ($r = 0.42 \pm 0.17$, $P < 0.01$ for 88 out of 94 sites). The response of $\frac{\mathrm{VOD_{daytime}}}{\mathrm{VOD_{nighttime}}}$ to soil water potential can also be used as a new metric for ecosystem iso/anisohydricity. Our study demonstrates that a large proportion of variations in VOD are caused by AGB for temperate ecosystems, and higher accuracy VOD products with additional root-zone soil water potential are needed for ecosystem iso/anisohydricity estimations.

1. Introduction

Microwave remote sensing has increasingly been used to obtain land-surface properties including surface soil moisture, surface roughness, snow and flood status, etc. (Njoku and Chan, 2006; Njoku and Entekhabi, 1996; Zhang and Armstrong, 2001). During the retrieval of surface soil moisture, vegetation is often treated as a semi-transparent layer that attenuates the microwave signal which can be quantitatively assessed by vegetation optical depth (VOD) (Owe et al., 2001). Previous studies have suggested that VOD can be interpreted as the total water content in all aboveground biomass (Liu et al., 2013). At higher frequencies, microwaves have less penetration into the vegetation and VOD is most sensitive to the upper part of the canopy, i.e., leaves and upper branches. Therefore, VOD retrieved at high frequencies (e.g., X-band, 10.7 GHz) is a good indicator for total water content in the upper canopy, and can be effectively used to monitoring canopy water content responses to drought (Anderegg et al., 2018). Due to the close linkage between leaf water content and leaf water potential, obtaining leaf water potential from microwave remote sensing is also promising.

Leaf water potential is an important variable in plant hydraulic and plant physiology research. The difference in water potential values between leaf and root provides the driving force of water movements in plants. Variation in leaf water potential is mostly caused by an imbalance between water consumption (transpiration) and supply (xylem

* Corresponding author. Department of Microbiology and Plant Biology, Center for Spatial Analysis, University of Oklahoma, Norman, OK, USA.
E-mail address: yaozhang@lbl.gov (Y. Zhang).

https://doi.org/10.1016/j.rse.2019.111451
Received 28 November 2018; Received in revised form 24 September 2019; Accepted 28 September 2019

transportation), while other processes, including the osmotic effect, might also contribute to the changes but to a lesser extent (Vesala et al., 2017). The dynamic changes of leaf water potential can be used to characterize plant water use strategy as a continuum from isohydry to anisohydry: more isohydric species tend to maintain a relatively steady daytime leaf water potential to prevent xylem embolism during drought while more anisohydric species tend to exhibit larger variations in terms of daytime leaf water potential (Tardieu and Simonneau, 1998). Although recent studies suggest that this definition is also affected by the environment and does not directly link to stomatal sensitivity to drought (Hochberg et al., 2018; Martínez-Vilalta and Garcia-Forner, 2017), it can still be used to characterize the leaf water dynamic to different drought stresses (atmospheric water deficit or soil water deficit) or as a constraint to benchmark plant hydraulic models (Kennedy et al., 2019). For example, Konings et al. (2017) demonstrates that in western US, more anisohydric grassland have higher sensitivity to atmospheric dryness than to soil dryness. Another study by Giardina et al. (2018) finds that in Amazon, tall trees are generally more isohydric and their photosynthesis are less sensitive to precipitation variability. Both studies avoid directly linking isohydricity metrics with plant species, and instead, focus on plant responses at ecosystem scale. Therefore, obtaining a global dataset of iso/anisohydricity can greatly benefit our understanding of plant physiological responses to drought and heat.

Based on the definition of iso/anisohydricity, Martínez-Vilalta et al. (2014) uses the regression slope (σ) between the midday leaf water potential (Ψ_L^{midday}) and predawn leaf water potential ($\Psi_L^{predawn}$) to represent plant iso/anisohydricity:

$$\Psi_L^{midday} = \sigma \Psi_L^{predawn} + \Lambda \quad (1)$$

This slope (σ) describes the capability of plants to maintain a relatively stable leaf water potential in response to declining soil water potential, and the intercept (Λ) indicates the Ψ_L^{midday} value when soil is fully saturated. It should be noted that other definitions of the iso/anisohydricity exist (e.g., difference of $\Psi_L^{predawn}$ and Ψ_L^{midday} within day (Klein, 2014), variations of Ψ_L^{midday}), which may not agree with each other (Martínez-Vilalta and Garcia-Forner, 2017). We here adopt the definition by Tardieu and Simonneau (1998). In practice, this method typically requires laborious field measurements and only works for individual plant or species, which limits its application at the ecosystem scale.

Konings and Gentine (2017) first implement this definition at ecosystem scale by assuming that satellite VOD can be used as a proxy of leaf water content, and further leaf water potential, so that the regression slope between daytime VOD and nighttime VOD can serve as a measurement of ecosystem iso/anisohydricity. Li et al. (2017) uses similar theory with multiple microwave remote sensing products (both active and passive), improving the isohydricity estimates at higher latitudes (Li et al., 2017). These studies provide estimates of global ecosystem iso/anisohydricity that can be used for ecosystem drought response analysis or model development (Konings et al., 2017).

However, questions arise with regards to the usage of VOD data. VOD is related to the total water content, which can be further decomposed into the aboveground biomass (AGB) and water content per biomass, with the latter regarded as a proxy of the leaf water potential. As a result, both the midday and midnight VOD are driven by seasonal changes of AGB and may not represent the difference between daytime and predawn leaf water potential (Guan et al., 2014; Jones et al., 2011). This directly affects the use of VOD to estimate ecosystem iso/anisohydricity as illustrated by Fig. 1 using an arbitrarily generated dataset. Although the changes in water content and AGB may affect each other, they respond to water deficit at different time scales. With high temporal resolution VOD data, their exclusive effects on VOD can be separated. Momen et al. (2017) build a model to separate the contribution of VOD using *in situ* measured leaf water potential and leaf area index (LAI, as a proxy of biomass). Based on ground observations at three forest sites, they find that including leaf water potential improved the prediction of VOD compared to using LAI alone, although these improvements are site-dependent. Whether and to what extent VOD is sensitive to leaf water potential needs to be further evaluated over more ecosystems with ground measurements. One obvious limitation is the uncertainties in VOD and AGB retrievals: even if we were able to remove the contribution from AGB, whether the leaf water potential estimated from VOD is sufficiently accurate to characterize ecosystem iso/anisohydricity is still unknown.

In this study, we aim to answer two questions that are critical to the usage of VOD to represent canopy water content (or leaf water potential) and to further estimate ecosystem iso/anisohydricity: (1) How much variation of VOD in the temporal domain can be explained by leaf water potential compared to AGB? (2) Is there an effective way to quantify leaf water potential dynamics using VOD without being contaminated by AGB? We used two independent VOD datasets from the Japan Aerospace Exploration Agency (JAXA) Advanced Microwave Scanning Radiometer-Earth Observing System (AMSR-E) together with the Oklahoma Mesonet climatological dataset to investigate VOD responses during soil moisture dry-down events.

2. Materials and methods

2.1. VOD relationship with NDVI and leaf water potential

When the frequency of electron magnetic wave increases, its penetration capability decreases. Microwave at X-band (10.7 GHz) can barely get through dense vegetation canopy layers and VOD retrieved at X-band is a proxy for total water in the vegetation canopy (or columnar vegetation water content, VWC, in kg m^{-2}) (Jackson and Schmugge, 1991; Jones et al., 2011). Although canopy structure and dielectric property may also affect the relationship between VOD and VWC, their effects are generally considered site-specific and time invariant (Jackson and Schmugge, 1991). In this study, we only focus on the seasonal dynamic of leaf water for each individual site, and the temporal variations of site-specific parameters are ignored. VWC is mostly affected by two factors:

(1) the aboveground biomass (AGB) or mostly leaf biomass. The seasonal dynamic of AGB is largely driven by leaf growth and senescence while contributions from stem and branch are relatively small (Dong et al., 2003; Liu et al., 2017). Leaf biomass or leaf area can be approximated using an exponential function or linear function of normalized difference vegetation index (NDVI) (Schino et al., 2003; Shippert et al., 1995; Wang et al., 2005). Previous studies suggest similar performances of these two models in deciduous and semi-arid ecosystems (Fan et al., 2009; Potithepa et al., 2010). For simplicity, we used a linear model to estimate AGB from NDVI:

$$AGB = q\text{NDVI} + u \quad (2)$$

It should be noted that we aim to predict the seasonal variation of AGB for each site instead of obtaining a universal relationship to predict the spatial pattern, this allows us to fit the q and u for each site individually.

(2) the average water content per unit of biomass (WC). WC is usually measured at leaf level and can be related to leaf water potential. The relationship between WC and leaf water potential can be complicated, since the latter is a combination of solute, pressure and gravity potential. Both solute potential and pressure potential are affected by the relative water content in the leaves (Nobel, 2009). Although solute potential can also be controlled by solute concentration adjustment, this effect is smaller and is ignored here (Wilson, 1967). Previous studies suggest either linear or non-linear relationship between leaf water content and leaf water potential,

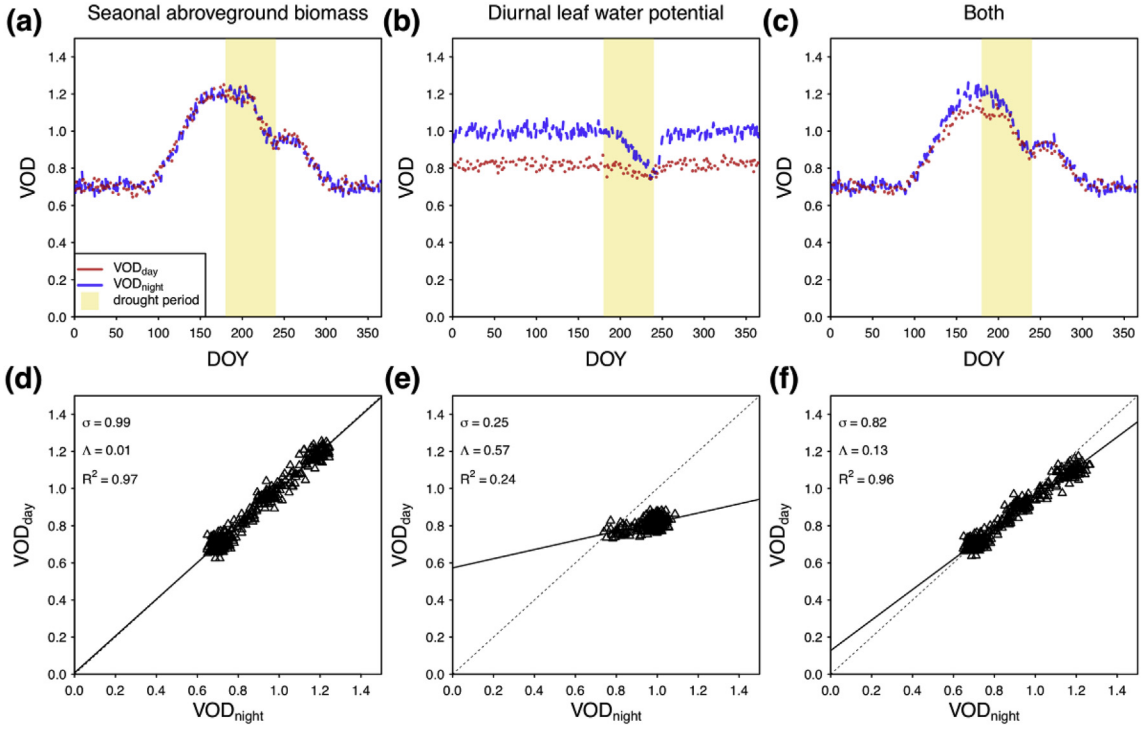

Fig. 1. Conceptualized representation of using satellite retrieved vegetation optical depth (VOD) to estimate ecosystem isohydricity with three different assumptions. (a,d) Assuming VOD variations are only affected by the seasonal changes of aboveground biomass (AGB); (b,e) Assuming VOD variation are only affected by the diurnal changes of the leaf water content (and therefore, leaf water potential); (c,f) Assuming VOD variations are affected by both AGB and leaf water content. The regression slope (σ) indicates whether the plants are more isohydric (close to 0) or anisohydric (close or great than 1). Data were arbitrarily generated with random noise embedded. Only the middle column correctly represents the conceptual framework proposed by Martínez-Vilalta et al. (2014), showing a more isohydric behavior, while under a real-world situation (right column), if the AGB contribution is not considered, regression slope close to one would indicate an anisohydric behavior.

depending on plant species (Jones and Higgs, 1979; Kalapos, 1994; Luo and Strain, 1992; Maxwell and Redmann, 1978; Sade, 2012; Zweifel et al., 2000). In our study, since we only used data with a narrow range of water potential variations, the linear approximation is adopted for simplicity (Pearcy, 1989):

$$\mathrm{WC} = m\Psi_L + n \tag{3}$$

q, u, m, n are empirical parameters that change in space but not over time, assuming they are still in the elastic part.

Following previous studies, VOD can be expressed as a combination of AGB and WC (Momen et al., 2017):

$$\mathrm{VOD} = \mathrm{b}(q\mathrm{NDVI} + u)(m\Psi_L + n) = \alpha + \beta\mathrm{NDVI} + \gamma\Psi_L + \eta\Psi_L\mathrm{NDVI} \tag{4}$$

The coefficients α, β, γ, η are assumed to only vary across sites and remain constant in time. We used a least square method to solve these coefficients for each site. In comparison, we also built two other models to investigate the VOD sensitivity to NDVI and Ψ_L respectively:

$$\mathrm{VOD} = \varkappa\,\mathrm{NDVI} + \mu \tag{5}$$

$$\mathrm{VOD} = \iota\Psi_L + \nu \tag{6}$$

where $\varkappa, \mu, \iota, \nu$ are also site level parameters that do not vary in the time domain.

Considering non-linear relationship between leaf water content and leaf water potential is also suggested in the literature, as well as the relationship between AGB and NDVI, it is necessary to test a model that is not restrained to these linearity assumptions. Here we also used the "boosted regression tree" (BRT) (Elith et al., 2008), a powerful machine learning tool to explore how much variance in VOD can be explained by NDVI and Ψ_L, and what is the contribution of each predictor variable. The BRT method combines the strength of "regression tree" method and "boosting ensembling" method. It can be regarded as an additive regression model in which each member ("a regression tree") are fitted in a forward, stepwise way. This machine learning approach does not require the linear assumption for both processes, and can handle complex interactive effects between leaf water potential and NDVI. By analyzing the tree complexity, it can also estimate the relative contribution of each predictor to the response variable from the fitted model. It should be noted that the contributions estimated from BRT are normalized and may not be directly comparable with that from the linear model, it is the relative relationship between the NDVI and Ψ_L contributions that we are interested in. The models were fitted at each site, using the R package "gbm" under R 3.6.1 environment.

2.2. Attributing the variation of VOD to NDVI and Ψ_L during soil moisture dry-down

We also used a variance decomposition method to separate the variance of VOD into contributions from NDVI, Ψ_L and NDVI × Ψ_L for the linear model (Eq. (4)). This method decomposes the variance of an aggregate variable into contributions of each component variable according to the covariance allocation principle (Zhou et al., 2017). In this study, the aggregate variable (VOD) consists of three component variables (α is constant) on the right-hand side in Eq. (4), and the variance of VOD is decomposed to its covariance with each component variable as follows:

$$VAR(\mathrm{VOD}) = cov(\mathrm{VOD},\ \beta\mathrm{NDVI}) + cov(\mathrm{VOD}, \gamma\Psi_L) + cov(\mathrm{VOD}, \eta\Psi_L\mathrm{NDVI}) + cov(\mathrm{VOD},\varepsilon) \tag{7}$$

where ε is the random error in the regression of Eq. (4). The explanatory power of NDVI, Ψ_L and the cross term NDVI × Ψ_L to variations in VOD (R_X) is given by:

$$R_X = \frac{cov(\mathrm{VOD},\ X)}{VAR(\mathrm{VOD})} \tag{8}$$

where X represents either βNDVI, $\gamma\Psi_L$ or $\eta\Psi_L$NDVI.

2.3. Ratio between daytime and nighttime VOD to eliminate the effect of aboveground biomass

Since the aboveground biomass does not change much over a short time period (e.g., within a few days) (Konings et al., 2016), the ratio between daytime VOD ($\mathrm{VOD_{day}}$) and nighttime VOD ($\mathrm{VOD_{night}}$) observations within one day (12 h apart) can eliminate the contribution from the aboveground biomass. Therefore, the ratio (R) between $\mathrm{VOD_{day}}$ and $\mathrm{VOD_{night}}$ can be regarded as the ratio between linear proxies of Ψ_L at midday and at midnight using Eq. (4):

$$R = \frac{\mathrm{VOD_{day}}}{\mathrm{VOD_{night}}} = \frac{m\Psi_L^{\mathrm{daytime}} + n}{m\Psi_L^{\mathrm{nighttime}} + n} \tag{9}$$

where m and n are site specific parameters as described in Eq. (3). Theoretically, by investigating the response of R to changing soil water conditions ($\Psi_L^{\mathrm{nighttime}}$), we can estimate vegetation iso/anisohydric behavior. Here we present a simple sensitivity analysis. Replace $\Psi_L^{\mathrm{daytime}}$ in Eq. (9) with Eq. (1) and we can get:

$$R = \frac{\mathrm{VOD_{day}}}{\mathrm{VOD_{night}}} = \frac{m\Psi_L^{\mathrm{daytime}} + n}{m\Psi_L^{\mathrm{nighttime}} + n} = \sigma + \frac{\Lambda + (1-\sigma)\mathrm{n/m}}{\Psi_L^{\mathrm{nighttime}} + n/m} \tag{10}$$

where σ is the regression slope between $\Psi_L^{\mathrm{daytime}}$ and $\Psi_L^{\mathrm{nighttime}}$ and is a metric of iso/anisohydricity (see introduction and Fig. 1). The first order derivative of R with respect to $\Psi_L^{\mathrm{nighttime}}$ represents the change of $\frac{\mathrm{VOD_{day}}}{\mathrm{VOD_{night}}}$ to $\Psi_L^{\mathrm{nighttime}}$:

$$\frac{dR}{d\Psi_L^{\mathrm{nighttime}}} = -\frac{\Lambda + (1-\sigma)\frac{n}{m}}{\left(\Psi_L^{\mathrm{nighttime}} + \frac{n}{m}\right)^2} \tag{11}$$

Considering $\left(\Psi_L^{\mathrm{nighttime}} + \frac{n}{m}\right)$ is always much greater than zero (m is positive, and $\mathrm{VOD} = m\Psi_L^{\mathrm{nighttime}} + n$ is always much greater than zero), and $\frac{n}{m}$ is much greater than $|\Lambda|$. The variation of $\frac{dR}{d\Psi_L^{\mathrm{nighttime}}}$ is dominated by the variation of numerator on the right-hand side of Eq. (11). When σ is close to or greater than 1 (more anisohydric), the numerator is negative, and $\frac{dR}{d\Psi_L^{\mathrm{nighttime}}}$ is positive. When σ is close to 0 (more isohydric), the numerator is positive, and $\frac{dR}{d\Psi_L^{\mathrm{nighttime}}}$ is negative. These mathematical derivations provide linkage between this new isohydricity metric and the widely used leaf level metric "σ".

2.4. Study area and Mesonet climate data

Oklahoma is in a transition zone from humid to arid climate and has a large variety of land cover types including forest, cropland, grassland, shrubland, etc. (Wang et al., 2018). A dry summer can often be expected due to the asynchronicity between temperature and precipitation (Flanagan et al., 2017). Oklahoma has experienced frequently drying conditions during the past decades (Ford et al., 2015), making it a suitable place to investigate the response of VOD to soil moisture dry-down.

Oklahoma Mesonet is a network of environmental monitoring stations, consisting of 141 sites quasi-evenly distributed over the state of Oklahoma (Fig. 2, Table S1). The Mesonet stations measure a variety of climate and environmental variables including temperature, precipitation, radiation, humidity, and soil water conditions (Brock et al., 1994; McPherson et al., 2007). For most sites, soil water conditions were measured at four soil depths (5 cm, 25 cm, 60 cm, 75 cm) using Campbell Scientific (CS) 229-L sensors (Campbell Scientific Inc. Logan, UT, USA) (Basara and Crawford, 2000). The CS 229-L sensor measures the temperature difference before and after a heat pulse is introduced, since the soil water content will affect the specific heat capacity, thermal conductivity and density of the porous median (ceramic matrix) where the sensor is housed, larger temperature difference is expected when soil is dry. Based on site calibrated coefficients, different soil water indicators can be calculated (see (Basara and Crawford, 2000)).

Soil water potential (Ψ_w) is not directly measured at Mesonet stations. However, as Ψ_w is a combination of both matric potential and solute potential, both of which decrease (become more negative) monotonically with soil drying, soil matric potential was used as a proxy of Ψ_w in this study (Or and Wraith, 2002). The soil matric potential was further used to represent predawn leaf water potential ($\Psi_L^{\mathrm{predawn}}$) when an equilibrium between soil water potential and leaf water potential is reached at predawn, and compared with VOD observations for descending overpass (1:30 a.m. local time, $\mathrm{VOD_{night}}$). It should be noted that there is a time difference between the satellite observation and predawn xylem refilling, and a disequilibrium is common for many species (Donovan et al., 2001, 2003). As long as a linear relationship exists between soil water potential and leaf water potential at 1:30 a.m. during a dry-down event (Bucci et al., 2004; Skelton et al., 2017; Williams and Araujo, 2002), soil matric potential can be linked to water content in a similar form as Eq. (3), and soil matric potential measurements can be used to test whether VOD is sensitive to leaf water potential changes during soil moisture dry-down.

In this study, soil matric potential depths at 25 cm were used to represent the root-zone soil water potential for non-forest sites, and averaged soil matric potential at 25 cm and 60 cm were used for forest sites. For each site, we calculated the land cover/use types from the National Land Cover Database (NLCD) for the 0.25° × 0.25° gridcells corresponding to the Mesonet stations (Boryan et al., 2011). Only forest or shrubland that occupy more than 50% of the gridcell for all three years (2001, 2006, 2011, so that the study period is covered) were considered as fully forested. Other land cover types (cropland, grassland) were considered as non-forested ecosystems. Sites with more than 10% of water body in the 0.25° × 0.25° gridcell were excluded using the NLCD dataset, since large water bodies affect VOD retrievals (Konings et al., 2016; Owe et al., 2008).

2.5. Soil moisture dry-down detection

We used the fractional water index (FWI) as an indicator of drought development. FWI can be directly calculated using the CS 229-L sensors:

$$\mathrm{FWI} = \frac{\Delta T_d - \Delta T_{ref}}{\Delta T_d - \Delta T_w} \tag{12}$$

where ΔT_d, ΔT_w, and ΔT_{ref} represent the normalized sensor response (in °C) under dry, wet and reference (measurement) conditions (Illston et al., 2008). With this normalization, FWI indicates the soil moisture between a range from 0 (dry soil) to 1 (saturated soil) (Sutherland and Illston, 2013; Schneider et al., 2003). We identified dry-down periods when FWI monotonically decreased over time: the initial FWI should be above 0.7, indicating a relatively abundant water supply; and the end FWI should be below 0.4, indicating water scarcity could have limited vegetation growth (Sutherland and Illston, 2013). FWI at 60 cm and 25 cm were used for forest and non-forest sites, respectively. Since the CS 229-L does not capture the matric potential during very dry conditions, we excluded the prolonged hyper arid condition when FWI is below 0.15 and the daily decrease of FWI is smaller than 0.002. Only dry-down periods longer than 15 days were used so that vegetation could have enough time to respond to the dryness. Altogether 1378 dry-down events were identified. 94 sites (7 forested, 87 non-forested) that

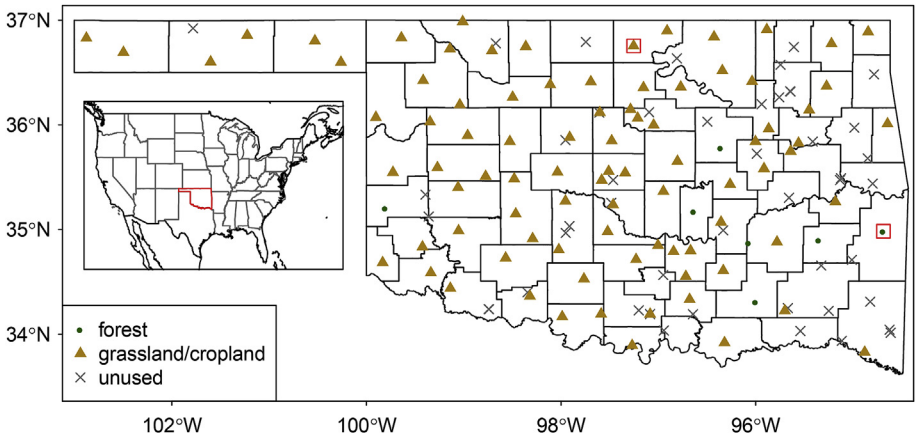

Fig. 2. Spatial distribution of the Mesonet stations in Oklahoma. The inset shows the location of Oklahoma in US. Symbols in different colors represent forest and non-forest ecosystem types. Two red boxes indicate the locations of two sites (Wister and Blackwell) that are used as examples as forested and non-forested in Fig. 3. (For interpretation of the references to color in this figure legend, the reader is referred to the Web version of this article.)

experienced at least one period of dry-down during 2003–2011 were used for the analysis (Table S1).

2.6. VOD data from LPRM and LPDR v2

Two VOD estimates from Advanced Microwave Scanning Radiometer-E (AMSR-E) sensor onboard Aqua Earth-observing satellite (EOS) were used in this study. The first VOD product is based on the Land Parameter Retrieval Model (LPRM) (Owe et al., 2008, 2001). Another VOD dataset is developed by the University of Montana (UMT) known as the Land Parameter Data Record version 2 (LPDR, hereafter) (Du et al., 2017). Compared to LPRM, the LPDR dataset uses a brightness temperature (T_b) calibrated against AMSR2 and a fractional water correction was implemented. The LPDR method also uses a temporal smoothing filter to remove the high frequency fluctuations. Both datasets cover the period 2003–2011 and were reprojected to latitude/longitude projection with a spatial resolution of 0.25° × 0.25°. Since X-band (10.7GHz) VOD is sensitive to the total water in the canopy, it is necessary to eliminate the contamination caused by precipitation interception by canopy. Days with precipitation from Mesonet greater than 1 mm in the previous 24-h were excluded. The quality-checked VOD was smoothed using a moving average filter with a window size of 5-days to remove the high frequency noises associated with measurement and retrieval algorithm uncertainties.

The Aqua satellite is on a sun-synchronous orbit and has two local overpass times within one day (1:30 a.m. local time for the descending node and 1:30 p.m. local time for the ascending node). In this study, both VOD retrievals were used and denoted as VOD_{day} (ascending node) and VOD_{night} (descending node), respectively.

2.7. Vegetation indices from MODIS

We used the 0.05° 16-day MODIS NDVI product (MOD13C1 C6) from 2002 to 2011 to represent vegetation cover conditions (Huete et al., 2002). The data quality was checked first, only pixels with good quality (MODLAND_QA = ”00″), low aerosol load (Aerosol quality = ”01″ or “10”), and good spatial coverage (Geospatial quality≠”00″) were used. Pixels that passed the quality check were averaged to the 0.25° × 0.25° gridcell to match the resolution of the VOD dataset. For each site, the 16-day NDVI values were interpolated into daily values with a spline interpolation to match the temporal resolution of VOD and soil water potential measurements from Mesonet.

3. Results

3.1. Linear model performance comparison

Fig. 3 shows the time series of meteorological and vegetation variables using one forested and one non-forested sites as examples. The light-yellow shades highlight the dry-down events that were identified by our algorithm. Compared to LPRM, LPDR VOD exhibits smaller high frequency fluctuations, which is likely caused by the temporal smoothing applied. However, the correlation between the two VOD datasets is still strong for both sites (Pearson's r = 0.75 and 0.65, respectively). The VOD_{day}/VOD_{night} ratio from the two datasets also shows similar time-series patterns for the entire growing season (Pearson's r = 0.50 and 0.55, respectively). All moisture dry-down events occur during the mid-growing season. For the forested site, the canopy biomass slightly decreases during the dry-down window; while for the non-forested site, the AGB exhibits larger variations, which may be caused by fire management or grazing. The rest of the study only uses the data during these dry-down windows to maximize the variation in soil water potential.

We then evaluated the performance of the three models proposed in section 2.1 for each Mesonet site. We used the midnight overpass observations from two VOD datasets as the response variables and NDVI and Ψ_L as predictor variables. The models that include both NDVI and leaf water potential (Ψ_L, approximated using soil matric potential) have the best performance with highest R^2 (0.33 and 0.51 for LPRM and LPDR, respectively), followed by the models that only use NDVI (0.27 and 0.46, respectively) (Fig. 4a). The models that only include Ψ_L exhibit very limited predictive power for most sites (< 0.10 on average). The R^2 is lower compared to Momen et al. (2017) mostly because the short study periods (only dry-down events) that also correspond to limited variations in AGB and VOD.

We also compared the NDVI and Ψ_L coefficients across these three models (Fig. 4b and c). The coefficients of NDVI for Ψ_L&NDVI model (β in Eq. (4)) are around 0.32 and 0.78 for LPRM and LPDR, respectively, slightly lower than that for the NDVI model (κ in Eq. (5)). The coefficient of Ψ_L is 0.39 (LPRM) and 0.52 (LPDR) for Ψ_L&NDVI model (γ in Eq. (4)), and close to zero for the Ψ_L model (ι in Eq. (6)). The LPDR dataset generally shows higher R^2 and NDVI coefficient compared to LPRM dataset. Model performance (R^2) and coefficients also show very large variances across different sites, with an average coefficient of variation 0.45 (R^2), 0.71 (NDVI coefficients), and 1.82 (Ψ_L coefficients), respectively. Momen et al. (2017) suggest that the intercept (α) in Eq. (4) maybe related to the biomass for the woody components, we also show higher α in forest than non-forest, but the difference is not significant ($P = 0.07$ for LPRM and $P = 0.24$ for LPDR using unpaired student's t-test). One possible explanation might be the different AGB indicators used (leaf area index or NDVI).

3.2. Contribution of NDVI, Ψ_L to VOD using the NDVI& Ψ_L model during soil moisture dry-down

Based on the variance decomposition method, we evaluated the

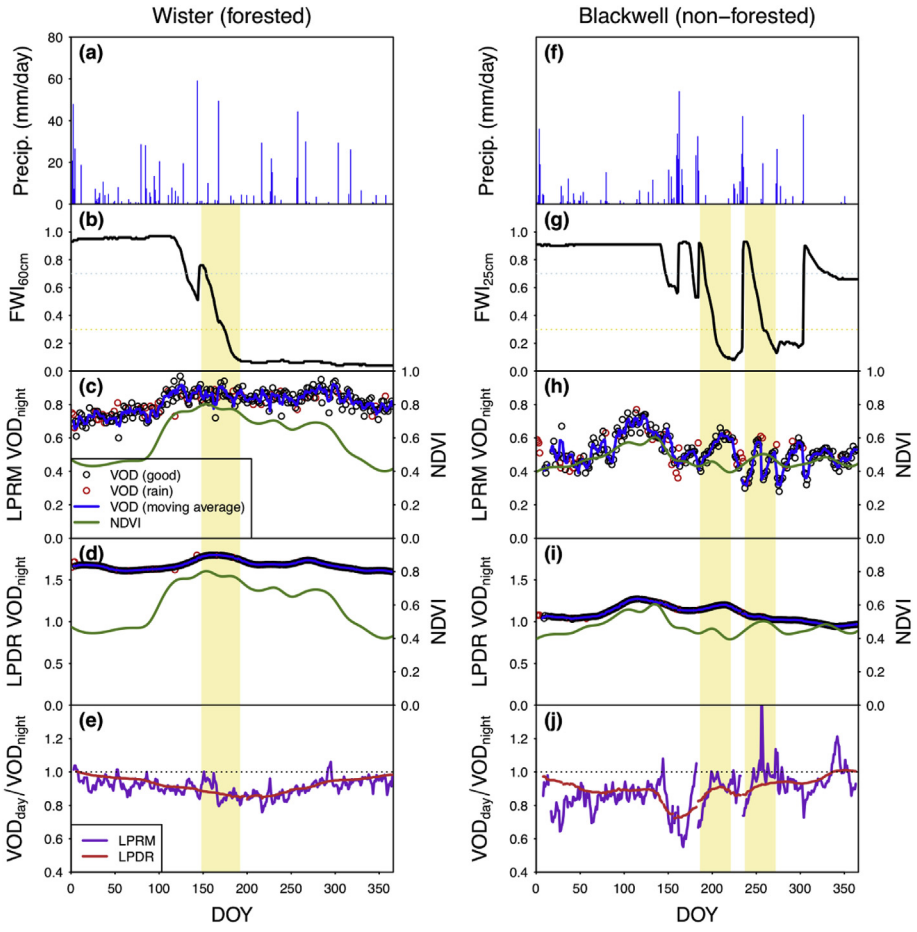

Fig. 3. Time series of precipitation (a, f), fractional water index (FWI) (b,g), LPRM VOD (c,h), LPDR VOD (d,i) and VOD_{day}/VOD_{night} for one forested site (Wister (longitude: 94.68778, latitude: 34.98426), 64% forest coverage) and one non-forested site (Blackwell (longitude: 97.25452, latitude: 36.75443), 0.3% forest coverage) for the year 2005.

contribution of each variable (NDVI, Ψ_L, $\Psi_L \times$ NDVI) on VOD in the Ψ_L &NDVI model for each site (Fig. 5). For most sites (61 out of 94 for LPRM and 76 out of 94 for LPDR), NDVI contributes most to the variance in the Ψ_L&NDVI model (0.24 on average for LPRM and 0.42 for LPDR). Ψ_L on average has smaller contribution than NDVI (0.18 for LPRM and 0.16 for LPDR), with contributions varying greatly across sites. The cross factor ($\Psi_L \times$ NDVI) contribution is negative in most sites. The Ψ_L contribution is greater in LPRM than the LPDR datasets, but the NDVI contribution is much higher in LPDR than LPRM. This difference may be related to the smoothing algorithm used in LPDR, which reduce the high frequency fluctuations caused by changes in leaf water content.

We further compared the contributions between forested and non-forested sites (Fig. 5). NDVI and Ψ_L contributions are generally higher for forested than non-forested sites for both VOD datasets. There are two possible explanations for this biome difference: (1) the soil moisture dry-down events in our study are mostly short-term and may not necessarily represent strong drought stress that may induce changes in AGB for grassland or forest, meaning that most of the AGB changes are caused by vegetation growth and senescence; (2) the X-band VOD used in this study is sensitive to total water in the upper canopy. Both forest and grassland have strong seasonal canopy dynamics, but considering the low biomass of the grassland, the signal to noise ratio may be higher in forest than grassland. This also leads to a generally higher model performance of the forest ($R^2 = 0.62 \pm 0.14$ for LPDR and $R^2 = 0.40 \pm 0.27$ for LPRM) than for non-forest ($R^2 = 0.50 \pm 0.18$ for LPDR and $R^2 = 0.33 \pm 0.17$ for LPRM) and higher contributions from the seasonal changes of AGB.

3.3. Relative contribution of NDVI and Ψ_L from machine learning models

The BRT model generally exhibits higher performance than the linear model (Fig. 6a and b). There is also a strong correlation between both model performances (R^2), suggesting that the major drivers for the model performance can be similar. We also compared the contribution of NDVI and Ψ_L between two models. Both models show higher contribution of NDVI than Ψ_L, which is also consistent across VOD datasets (Fig. 6c and d). The contributions of NDVI from both models are also strongly correlated ($r = 0.71$ and 0.69 for LPRM and LPDR, respectively), while the correlation between the Ψ_L contributions are not significant ($P = 0.46$ and 0.09 for LPRM and LPDR, respectively). This indicates the Ψ_L effects on VOD can be complicated, further highlighting the importance of our study.

3.4. Response of daytime leaf water potential vs. nighttime leaf water potential as soil dries

We have shown that VOD variations during the soil dry-downs are dominated by changes in AGB represented by NDVI. We calculate the ratio between VOD_{day} and VOD_{night} to eliminate the AGB contribution (Eq. (9), Fig. 3 e,j). This ratio is further evaluated against soil matric potential to explore its response to decreases in soil water potential. Here we use two sites as examples where dominant species are known (Fig. 7). VOD_{day}/VOD_{night} calculated from two VOD datasets shows strong correlation ($r = 0.30$, $P < 0.001$ for Wister, and $r = 0.69$, $P < 0.001$ for Blackwell). VOD_{day}/VOD_{night} and soil matric potential shows positive correlation for Wister but negative correlation for Blackwell. Although the two VOD datasets yield different regression slopes, the general patterns (decrease or increase) are consistent. These results suggest that after AGB information is removed by calculating the

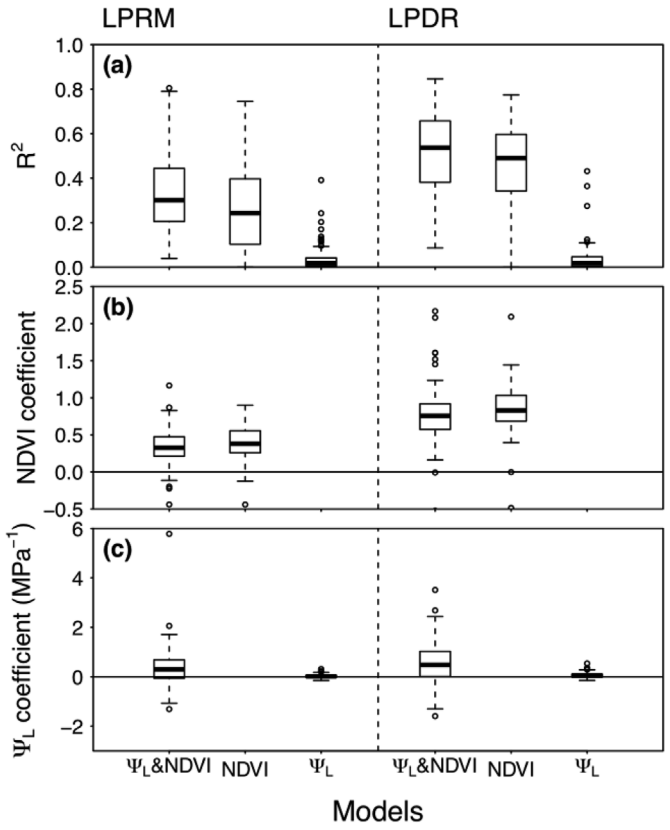

Fig. 4. Comparison between (a) the model coefficient of determination (R^2), (b) NDVI coefficient (β or κ) and (c) Ψ_L coefficient (γ or ι) for Ψ_L&NDVI model, NDVI model and Ψ_L model for both LPRM VOD and LPDR VOD. Since both VOD and NDVI are unitless, the unit for NDVI coefficient is also unitless and the unit for Ψ_L coefficient is (MPa^{-1}).

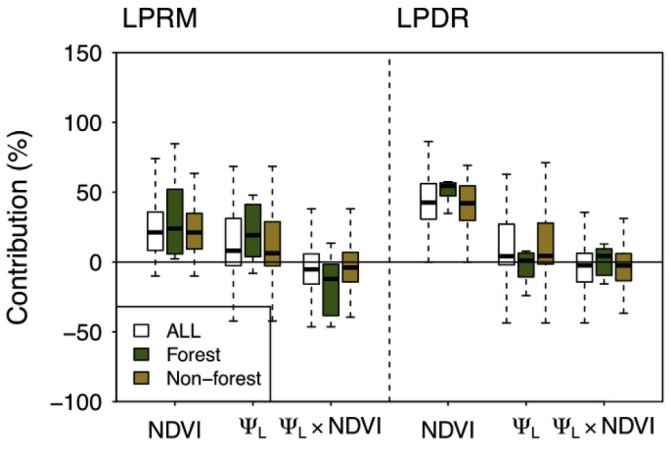

Fig. 5. Comparison between the contribution from NDVI, Ψ_L and the combined effect of NDVI and Ψ_L ($\Psi_L \times$ NDVI) for the Ψ_L&NDVI model for forested (green), non-forested (brown) and all sites (white). (For interpretation of the references to color in this figure legend, the reader is referred to the Web version of this article.)

ratio between VOD_{day} and VOD_{night}, the residuals still contain leaf water potential information. Results from both VOD datasets are consistent with each other.

When we extend this analysis to all Mesonet sites, VOD_{day}/VOD_{night} estimates from two datasets shows strong correlations for most of sites ($r = 0.42 \pm 0.17$, $P < 0.01$ for 88 out of 94 sites). Around two thirds of the sites (64 out of 94 for LPRM and 52 out of 94 for LPDR) show negative correlations between VOD_{day}/VOD_{night} and soil matric

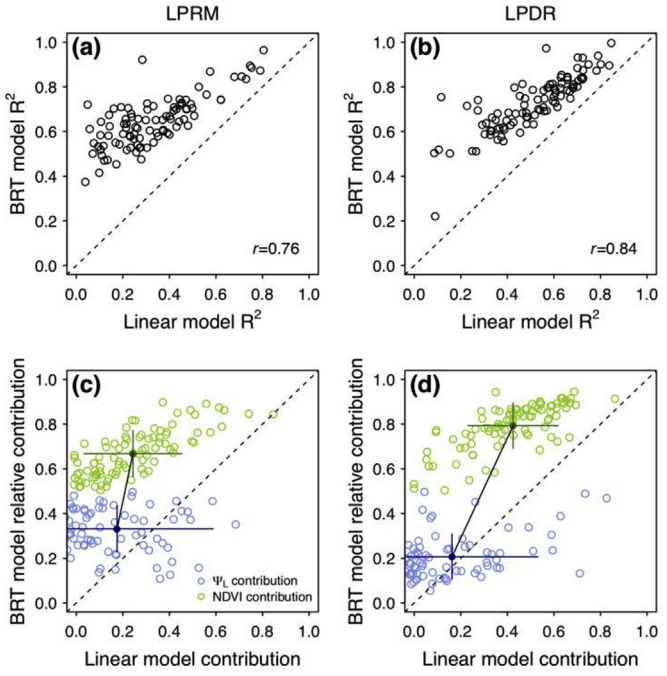

Fig. 6. Comparison of model performance (upper panel) and predictor contribution (bottom panel) between BRT model and linear model. Each point in (a) and (b) represents the model fitted based on all dry-down events for one site. Each point in (c) and (d) represents the contribution of either Ψ_L (blue) or NDVI (green) for one site. The blue and green dots with horizontal and vertical bars indicate the average and standard deviation of contribution from all sites. Left column uses VOD from LPRM and right column uses VOD from LPDR. (For interpretation of the references to color in this figure legend, the reader is referred to the Web version of this article.)

potential (Fig. 8). When comparing these two datasets against each other, VOD_{day}/VOD_{night} from both datasets have similar correlation coefficients (Fig. 8c). However, the regression slopes are slightly greater for LPRM than for LPDR, consistent with our two-site analyses shown in Fig. 7. Forested and non-forested sites do not exhibit a significant difference in terms of both correlation coefficients and regression slopes.

4. Discussion and conclusions

Both leaf water potential and aboveground biomass change over time, and their variations are not fully independent from each other, making it difficult to interpret the information embedded in VOD variations during soil moisture dry-down events. By investigating the midnight VOD variations during the dry-down periods, which correspond to a relatively larger change in Ψ_L (from close to 0 to very negative), NDVI shows higher correlation with VOD than Ψ_L, and exhibits a larger contribution to the variation of VOD for most sites. Our results are consistent with a recent study using the direct measurements of predawn leaf water potential (Momen et al., 2017).

Since AGB contributes a large proportion of temporal variation in VOD even during the dry-down periods when the soil water potential changes enormously, failing to account for AGB variations directly affects the retrieval of the ecosystem iso/anisohydricity (Fig. 1). For temperate ecosystems or ecosystems with strong seasonality, the VOD variation is thus dominated by the phenology of the vegetation. Previous methods (e.g., Konings and Gentine (2017) and Li et al. (2017)) that use the regression between midday and midnight VOD observations would exert stronger linear correlation in these regions, resulting in a prediction of more anisohydric ecosystem (regression slope ≈ 1) (Fig. 1c). While for evergreen ecosystems, the VOD variations in time are less affected by the change of AGB; the uncertainty of VOD as well

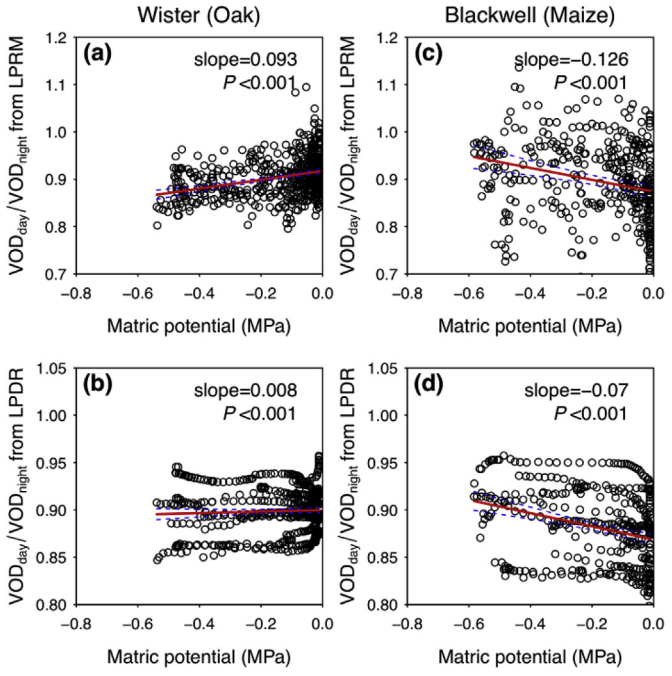

Fig. 7. Responses of VOD_{day}/VOD_{night} from LPRM (a, c) and LPDR (b, d) during soil dry-down events. One forest site (Wister, left column) and one non-forest site (Blackwell, right column) are shown as examples. Wister is located in the southeast Oklahoma and is dominated by oak forest (Diamond and Elliot, 2015); Blackwell is dominated by cropland with maize occupies 24% of the VOD pixel (0.25° × 0.25°) according to the cropland data layer (CDL-USDA) dataset (https://nassgeodata.gmu.edu/CropScape/). The red lines represent the linear regression, and the blue dashed lines represents the 95% confidence intervals for the regression. (For interpretation of the references to color in this figure legend, the reader is referred to the Web version of this article.)

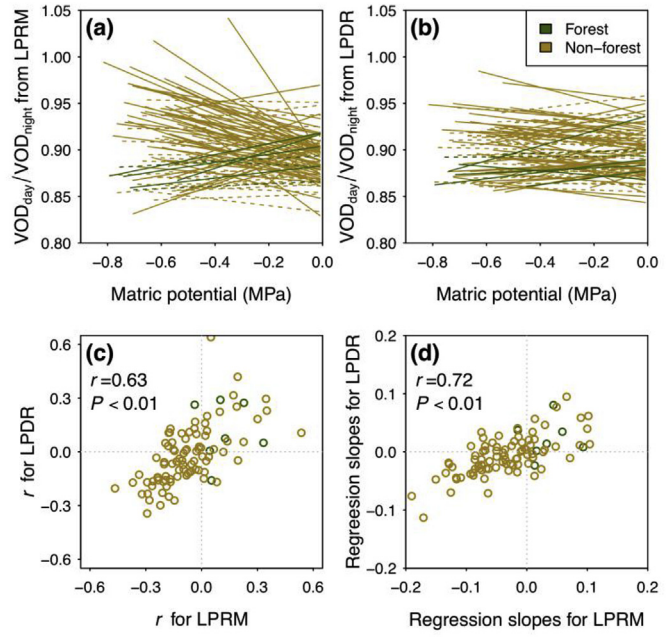

Fig. 8. Relationship between the soil matric potential and the daytime VOD/nighttime VOD from LPRM (a) and LPDR (b). Each line represents the regression for one site. Solid lines indicate the regression is significant with a *P*-value of 0.05. Comparison between the two VOD datasets in terms of correlation coefficient (c) and regression slope (d).

as the change in Ψ_L may contribute to a larger proportion of the VOD variation, leading to a prediction of more isohydric ecosystem. Recent studies suggested that at the species level, the iso/anisohydricity may be unrelated to vegetation seasonality (Braga et al., 2016; Cardoso et al., 2015). Therefore, the contribution of AGB to VOD should be eliminated when estimating ecosystem iso/anisohydricity. We suggest that using the ratio of VOD_{day}/VOD_{night} and its response to soil water potential is a better indicator of iso/anisohydricity as it is unaffected by changes in biomass.

For isohydric species, plants tend to maintain a constant daytime leaf water potentials against decreasing soil water potential (Martínez-Vilalta and Garcia-Forner, 2017; Martínez-Vilalta et al., 2014). Therefore, the VOD_{day}/VOD_{night} ratio increases when soil dries down (Fig. 9a). For anisohydric species, the daytime leaf water potential decreases along with the decreasing soil water potential, and we expect to see the ratio to be constant or slightly decreasing with soil dry-down (Fig. 9c). Subsequently, the regression slope between VOD_{day}/VOD_{night} vs. root zone soil water content can be used as a new metric for ecosystem iso/anisohydricity. Our mathematical derivation also demonstrates the direct linkage between this new metric and the widely used "σ". The metric derived for 94 Mesonet stations is also highly consistent using both VOD datasets (Fig. 8d). This indicator has the advantage over previous ones by taking the dynamic change in AGB into consideration. Using two Mesonet sites as examples, Blackwell shows a negative regression slope and can be regarded being more isohydric, while Wister exhibits a positive regression slope corresponding to a more anisohydric behavior (Fig. 7). These estimates are also consistent with the species composition of the two sites. Oak in Wister is more anisohydric while maize in Blackwell tend to be more isohydric (Tardieu et al., 1993; Yi et al., 2017).

However, as has been shown in our results section, a proportion of variations in VOD cannot be explained by either the AGB or the WC. These unexplained variations may be related to the uncertainty of the VOD retrieval or the linearity assumptions used (see detailed description in Method Section 2.1 and 2.4). Considering the natural spatial heterogeneity of soil moisture (due to landscape and rainfall heterogeneity), the Mesonet measured soil matric potential may not accurately represent the average conditions for the VOD pixel. This mismatch of measurement footprint also contributes to the uncertainties in our analysis. Different VOD retrieval methods (LPRM or LPDR) does not show significant improvements in reducing these uncertainties. These uncertainties directly affect the calculation of the VOD_{day}/VOD_{night} ratio, and further the regression slopes. It should be noted that similar to previous studies, the metric proposed in this study is also affected by the microwave band used for VOD retrieval. The higher frequency microwaves penetrate less in the vegetation canopy and can reflect the changes of water mostly in the upper canopy (Jones et al., 2011; Konings and Gentine, 2017; Momen et al., 2017; Tian et al., 2018), but they are also more sensitive to rainfall and dew. With decreasing microwave frequency, VOD contains more information of the total vegetation water in the branches and stems, as well as the understory vegetation; the relative sensitivity to the leaf water content decreases, and so will the model performance. Due to limitations in data availability, the model presented in this study is not tested using even higher frequency VOD dataset (e.g., K-band at 19 GHz). This can be done in future studies. In addition, this metric requires root-zone soil moisture estimates that cannot be directly derived from concurrent active and passive remote sensing. This limits its application at a regional or global scale. However, with the extensive soil moisture measurements networks (e.g., International Soil Moisture Network (ISMN), FLUXNET), ecosystem iso/anisohydricity can be effectively retrieved at these sites where leaf water potential measurements are missing. Lastly, recent development in satellite remote sensing and data assimilation techniques will also improve the accuracy of global root-zone soil moisture datasets and help generate contiguous dataset.

A global iso/anisohydricity dataset is important for understanding

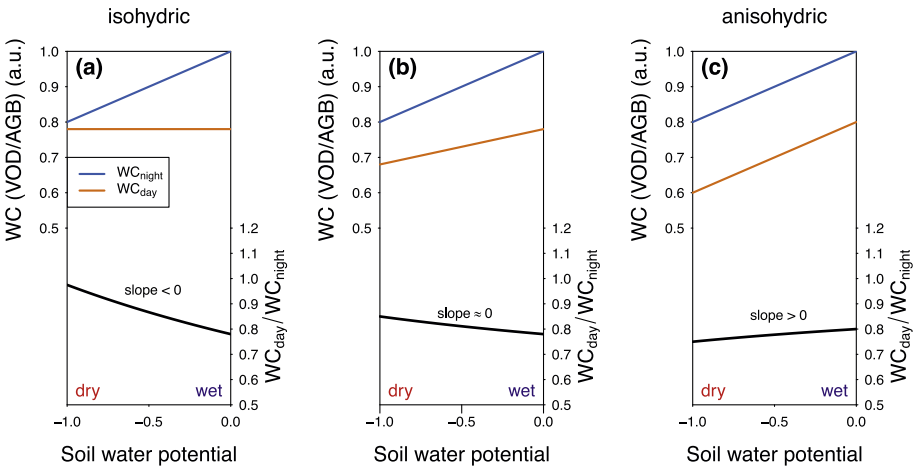

Fig. 9. Conceptual representation of water content (WC) variation during a dry down period for (a) an isohydric ecosystem (c) an anisohydric ecosystem and (b) an ecosystem with intermediate behavior. The WC_{day}/WC_{night} can be calculated as VOD_{day}/VOD_{night}. The regression slope between WC_{day}/WC_{night} and root-zone soil water potential can be used to assess ecosystem iso/anisohydricity.

ecosystem responses to drought and climate change, and further incorporate hydraulic processes into land surface models. By comparing two VOD datasets against the soil matric potential from the Mesonet stations with various vegetation and climate condition, our results suggest that the use of VOD to estimate ecosystem iso/anisohydricity is hindered by the fact that VOD variation is dominated by AGB. A new metric is proposed and is not affected by the seasonal variation of AGB. Since a global estimate of leaf water potential is not possible at present, increasing the VOD dataset accuracy and obtaining a global root-zone soil water potential (or soil water content) is imperative to get better ecosystem iso/anisohydricity estimates. More *in situ* and high frequency observations of leaf water potential are also needed to directly validate the VOD sensitivity to AGB and leaf water potential and the iso/anisohydricity derived from different methods.

Acknowledgements

We thank Dr. Jeffrey Basara from the University of Oklahoma for providing the Mesonet dataset. We also thank NASA GES DISC and NTSG at the University of Montana for providing the VOD dataset. We appreciate early discussion with Dr. Yan Li at University of Illinois Urbana Champaign. We also thank Brianna R. Pagán for English language editing. This study is partially supported by a research grant (Project No. 2013-69002-23146 and 2016-68002-24967) through the USDA National Institute for Food and Agriculture (NIFA), a research grant (IIA-1301789) from the National Science Foundation EPSCoR.

Appendix A. Supplementary data

Supplementary data to this article can be found online at https://doi.org/10.1016/j.rse.2019.111451.

References

Anderegg, W.R.L., Konings, A.G., Trugman, A.T., Yu, K., Bowling, D.R., Gabbitas, R., Karp, D.S., Pacala, S., Sperry, J.S., Sulman, B.N., Zenes, N., 2018. Hydraulic diversity of forests regulates ecosystem resilience during drought. Nature 1. https://doi.org/10.1038/s41586-018-0539-7.

Basara, J.B., Crawford, T.M., 2000. Improved installation procedures for deep-layer soil moisture measurements. J. Atmos. Ocean. Technol. 17, 879–884. https://doi.org/10.1175/1520-0426(2000)017<0879:IIPFDL>2.0.CO;2.

Boryan, C., Yang, Z., Mueller, R., Craig, M., 2011. Monitoring US agriculture: the US department of agriculture, national agricultural statistics service, cropland data layer program. Geocarto Int. 26, 341–358. https://doi.org/10.1080/10106049.2011.562309.

Braga, N. da S., Vitória, A.P., Souza, G.M., Barros, C.F., Freitas, L., 2016. Weak relationships between leaf phenology and isohydric and anisohydric behavior in lowland wet tropical forest trees. Biotropica 48, 453–464. https://doi.org/10.1111/btp.12324.

Brock, F.V., Crawford, K.C., Elliott, R.L., Cuperus, G.W., Stadler, S.J., Johnson, H.L., Eilts, M.D., 1994. The Oklahoma Mesonet: a technical overview. J. Atmos. Ocean. Technol. 12, 5–19. https://doi.org/10.1175/1520-0426(1995)012<0005:TOMATO>2.0.CO;2.

Bucci, S.J., Scholz, F.G., Goldstein, G., Meinzer, F.C., Hinojosa, J.A., Hoffmann, W.A., Franco, A.C., 2004. Processes preventing nocturnal equilibration between leaf and soil water potential in tropical savanna woody species. Tree Physiol. 24, 1119–1127.

Cardoso, J.A., Pineda, M., Jiménez, Juan de la Cruz, Vergara, M.F., Rao, I.M., 2015. Contrasting strategies to cope with drought conditions by two tropical forage C4 grasses. AoB Plants 7, plv107. https://doi.org/10.1093/aobpla/plv107.

Dong, J., Kaufmann, R.K., Myneni, R.B., Tucker, C.J., Kauppi, P.E., Liski, J., Buermann, W., Alexeyev, V., Hughes, M.K., 2003. Remote sensing estimates of boreal and temperate forest woody biomass: carbon pools, sources, and sinks. Remote Sens. Environ. 84, 393–410. https://doi.org/10.1016/S0034-4257(02)00130-X.

Donovan, L., Linton, M., Richards, J., 2001. Predawn plant water potential does not necessarily equilibrate with soil water potential under well-watered conditions. Oecologia 129, 328–335. https://doi.org/10.1007/s004420100738.

Donovan, L.A., Richards, J.H., Linton, M.J., 2003. Magnitude and mechanisms of disequilibrium between predawn plant and soil water potentials. Ecology 84, 463–470. https://doi.org/10.1890/0012-9658(2003)084[0463:MAMODB]2.0.CO;2.

Du, J., Kimball, J.S., Jones, L.A., Kim, Y., Glassy, J., Watts, J.D., 2017. A global satellite environmental data record derived from AMSR-E and AMSR2 microwave Earth observations. Earth Syst. Sci. Data 9, 791–808. https://doi.org/10.5194/essd-9-791-2017.

Elith, J., Leathwick, J.R., Hastie, T., 2008. A working guide to boosted regression trees. J. Anim. Ecol. 77, 802–813. https://doi.org/10.1111/j.1365-2656.2008.01390.x.

Fan, L., Gao, Y., Brück, H., Bernhofer, Ch, 2009. Investigating the relationship between NDVI and LAI in semi-arid grassland in Inner Mongolia using in-situ measurements. Theor. Appl. Climatol. 95, 151–156. https://doi.org/10.1007/s00704-007-0369-2.

Flanagan, P.X., Basara, J.B., Xiao, X., 2017. Long-term analysis of the asynchronicity between temperature and precipitation maxima in the United States Great Plains. Int. J. Climatol. 37, 3919–3933. https://doi.org/10.1002/joc.4966.

Ford, T.W., McRoberts, D.B., Quiring, S.M., Hall, R.E., 2015. On the utility of in situ soil moisture observations for flash drought early warning in Oklahoma, USA. Geophys. Res. Lett. 42, 9790–9798. https://doi.org/10.1002/2015GL066600.

Giardina, F., Konings, A.G., Kennedy, D., Alemohammad, S.H., Oliveira, R.S., Uriarte, M., Gentine, P., 2018. Tall Amazonian forests are less sensitive to precipitation variability. Nat. Geosci. 1. https://doi.org/10.1038/s41561-018-0133-5.

Guan, K., Wood, E.F., Medvigy, D., Kimball, J., Pan, M., Caylor, K.K., Sheffield, J., Xu, X., Jones, M.O., 2014. Terrestrial hydrological controls on land surface phenology of African savannas and woodlands. J. Geophys. Res. G Biogeosci. 119, 1652–1669. https://doi.org/10.1002/2013JG002572.

Hochberg, U., Rockwell, F.E., Holbrook, N.M., Cochard, H., 2018. Iso/anisohydry: a plant–environment interaction rather than a simple hydraulic trait. Trends Plant Sci. 23, 112–120. https://doi.org/10.1016/j.tplants.2017.11.002.

Huete, A., Didan, K., Miura, T., Rodriguez, E.P., Gao, X., Ferreira, L.G., 2002. Overview of the radiometric and biophysical performance of the MODIS vegetation indices. Remote Sens. Environ. 83, 195–213. https://doi.org/10.1016/S0034-4257(02)00096-2. The Moderate Resolution Imaging Spectroradiometer (MODIS): a new generation of Land Surface Monitoring.

Jackson, T.J., Schmugge, T.J., 1991. Vegetation effects on the microwave emission of soils. Remote Sens. Environ. 36, 203–212. https://doi.org/10.1016/0034-4257(91)90057-D.

Jones, H.G., Higgs, K.H., 1979. Water Potential-Water Content Relationships In Apple Leaves. Journal of Experimental Botany 30 (5), 965–970 In this issue.

Jones, M.O., Jones, L.A., Kimball, J.S., McDonald, K.C., 2011. Satellite passive microwave remote sensing for monitoring global land surface phenology. Remote Sens. Environ. 115, 1102–1114. https://doi.org/10.1016/j.rse.2010.12.015.

Kalapos, T., 1994. Leaf water potential-leaf water deficit relationship for ten species of a semiarid grassland community. Plant and Soil 160 (1), 105–112. https://doi.org/10.1007/BF00150351. In this issue.

Kennedy, D., Swenson, S., Oleson, K.W., Lawrence, D.M., Fisher, R., Costa, A.C.L. da, Gentine, P., 2019. Implementing plant hydraulics in the community land model, version 5. J. Adv. Model. Earth Syst. 11, 485–513. https://doi.org/10.1029/

2018MS001500.
Klein, T., 2014. The variability of stomatal sensitivity to leaf water potential across tree species indicates a continuum between isohydric and anisohydric behaviours. Funct. Ecol. 28, 1313–1320. https://doi.org/10.1111/1365-2435.12289.
Konings, A.G., Gentine, P., 2017. Global variations in ecosystem-scale isohydricity. Glob. Chang. Biol. 23, 891–905. https://doi.org/10.1111/gcb.13389.
Konings, A.G., Piles, M., Rötzer, K., McColl, K.A., Chan, S.K., Entekhabi, D., 2016. Vegetation optical depth and scattering albedo retrieval using time series of dual-polarized L-band radiometer observations. Remote Sens. Environ. 172, 178–189. https://doi.org/10.1016/j.rse.2015.11.009.
Konings, A.G., Williams, A.P., Gentine, P., 2017. Sensitivity of grassland productivity to aridity controlled by stomatal and xylem regulation. Nat. Geosci. 10, 284–288. https://doi.org/10.1038/ngeo2903.
Li, Y., Guan, K., Gentine, P., Konings, A.G., Meinzer, F.C., Kimball, J.S., Xu, X., Anderegg, W.R.L., McDowell, N.G., Martinez-Vilalta, J., Long, D.G., Good, S.P., 2017. Estimating global ecosystem isohydry/anisohydry using active and passive microwave satellite data. J. Geophys. Res. Biogeosci. 122. https://doi.org/10.1002/2017JG003958.
Liu, S., Cheng, F., Dong, S., Zhao, H., Hou, X., Wu, X., 2017. Spatiotemporal dynamics of grassland aboveground biomass on the Qinghai-Tibet Plateau based on validated MODIS NDVI. Sci. Rep. 7, 4182. https://doi.org/10.1038/s41598-017-04038-4.
Liu, Y.Y., van Dijk, A.I.J.M., McCabe, M.F., Evans, J.P., de Jeu, R.A.M., 2013. Global vegetation biomass change (1988-2008) and attribution to environmental and human drivers. Glob. Ecol. Biogeogr. 22, 692–705. https://doi.org/10.1111/geb.12024.
Luo, Y.-H., Strain, B.R., 1992. Alteration of Components of Leaf Water Potential and Water Content in Velvetleaf under the Effects of Long-Term Humidity Difference. Plant Physiology 98 (3), 966–970 In this issue.
Martínez-Vilalta, J., Garcia-Forner, N., 2017. Water potential regulation, stomatal behaviour and hydraulic transport under drought: deconstructing the iso/anisohydric concept. Plant Cell Environ. 40, 962–976. https://doi.org/10.1111/pce.12846.
Martínez-Vilalta, J., Poyatos, R., Aguade, D., Retana, J., Mencuccini, M., 2014. A new look at water transport regulation in plants. New Phytol. 204, 105–115. https://doi.org/10.1111/nph.12912.
Maxwell, J.O., Redmann, R.E., 1978. Leaf water potential, component potentials and relative water content in a xeric grass, Agropyron dasystachyum (Hook.) Scribn. Oecologia 35 (3), 277–284. https://doi.org/10.1007/BF00345136. In this issue.
McPherson, R.A., Fiebrich, C.A., Crawford, K.C., Kilby, J.R., Grimsley, D.L., Martinez, J.E., Basara, J.B., Illston, B.G., Morris, D.A., Kloesel, K.A., Melvin, A.D., Shrivastava, H., Wolfinbarger, J.M., Bostic, J.P., Demko, D.B., Elliott, R.L., Stadler, S.J., Carlson, J.D., Sutherland, A.J., 2007. Statewide monitoring of the mesoscale environment: a technical update on the Oklahoma Mesonet. J. Atmos. Ocean. Technol. 24, 301–321. https://doi.org/10.1175/JTECH1976.1.
Momen, M., Wood, J.D., Novick, K.A., Pangle, R., Pockman, W.T., McDowell, N.G., Konings, A.G., 2017. Interacting effects of leaf water potential and biomass on vegetation optical depth. J. Geophys. Res. Biogeosci. 122, 3031–3046. https://doi.org/10.1002/2017JG004145.
Njoku, E.G., Chan, S.K., 2006. Vegetation and surface roughness effects on AMSR-E land observations. Remote Sens. Environ. 100, 190–199. https://doi.org/10.1016/j.rse.2005.10.017.
Njoku, E.G., Entekhabi, D., 1996. Passive microwave remote sensing of soil moisture. J. Hydrol. Soil Moisture Theor. Observ. 184, 101–129. https://doi.org/10.1016/0022-1694(95)02970-2.
Nobel, P.S., 2009. Physicochemical and Environmental Plant Physiology. Elsevier.
Or, D., Wraith, J.M., 2002. Soil water content and water potential relationships. Soil Phys. Companion 1, 49–84.
Owe, M., de Jeu, R., Holmes, T., 2008. Multisensor historical climatology of satellite-derived global land surface moisture. J. Geophys. Res. Earth Surf. 113, F01002. https://doi.org/10.1029/2007JF000769.
Owe, M., Jeu, R. de, Walker, J., 2001. A methodology for surface soil moisture and vegetation optical depth retrieval using the microwave polarization difference index. IEEE Trans. Geosci. Remote Sens. 39, 1643–1654. https://doi.org/10.1109/36.942542.
Pearcy, R.W., 1989. Field data acquisition. Plant Physiological Ecology. Springer, Dordrecht, pp. 15–27.
Potithepa, S., Nasaharab, N.K., Muraokac, H., Nagaia, S., Suzukia, R.O., 2010. What IS the actual relationship between LAI and VI IN a deciduous broadleaf FOREST ? International Archives of the Photogrammetry, Remote Sensing and Spatial Information Science.
Sade, N., et al., 2012. Risk-taking plants. Plant Signaling & Behavior 7 (7), 767–770. https://doi.org/10.4161/psb.20505. In this issue.
Schino, G., Borfecchia, F., De Cecco, L., Dibari, C., Iannetta, M., Martini, S., Pedrotti, F., 2003. Satellite estimate of grass biomass in a mountainous range in central Italy. Agrofor. Syst. 59, 157–162. https://doi.org/10.1023/A:1026308928874.
Shippert, M.M., Walker, D.A., Auerbach, N.A., Lewis, B.E., 1995. Biomass and leaf-area index maps derived from SPOT images for Toolik Lake and Imnavait Creek areas, Alaska. Polar Rec. 31, 147–154. https://doi.org/10.1017/S0032247400013644.
Skelton, R.P., Brodribb, T.J., McAdam, S.A.M., Mitchell, P.J., 2017. Gas exchange recovery following natural drought is rapid unless limited by loss of leaf hydraulic conductance: evidence from an evergreen woodland. New Phytol. 215, 1399–1412. https://doi.org/10.1111/nph.14652.
Sutherland, A., Illston, B.G., 2013. Fractional water indexhttps://www.mesonet.org/images/site/Fractional%20Water%20Index%20User%20Info%20Aug2013.pdf accessed 21 March 2018.
Tardieu, F., Simonneau, T., 1998. Variability among species of stomatal control under fluctuating soil water status and evaporative demand: modelling isohydric and anisohydric behaviours. J. Exp. Bot. 49, 419–432.
Tardieu, F., Zhang, J., Gowing, D.J.G., 1993. Stomatal control by both [ABA] in the xylem sap and leaf water status: a test of a model for draughted or ABA-fed field-grown maize. Plant Cell Environ. 16, 413–420. https://doi.org/10.1111/j.1365-3040.1993.tb00887.x.
Tian, F., Wigneron, J.-P., Ciais, P., Chave, J., Ogée, J., Peñuelas, J., Ræbild, A., Domec, J.-C., Tong, X., Brandt, M., Mialon, A., Rodriguez-Fernandez, N., Tagesson, T., Al-Yaari, A., Kerr, Y., Chen, C., Myneni, R.B., Zhang, W., Ardö, J., Fensholt, R., 2018. Coupling of ecosystem-scale plant water storage and leaf phenology observed by satellite. Nat. Ecol. Evol. 1. https://doi.org/10.1038/s41559-018-0630-3.
Vesala, T., Sevanto, S., Grönholm, T., Salmon, Y., Nikinmaa, E., Hari, P., Hölttä, T., 2017. Effect of leaf water potential on internal humidity and CO2 dissolution: reverse transpiration and improved water use efficiency under negative pressure. Front. Plant Sci. 8. https://doi.org/10.3389/fpls.2017.00054.
Wang, J., Xiao, X., Zhang, Y., Qin, Y., Doughty, R.B., Wu, X., Bajgain, R., Du, L., 2018. Enhanced gross primary production and evapotranspiration in juniper encroached grasslands. Glob. Chang. Biol. 0. https://doi.org/10.1111/gcb.14441.
Wang, Q., Adiku, S., Tenhunen, J., Granier, A., 2005. On the relationship of NDVI with leaf area index in a deciduous forest site. Remote Sens. Environ. 94, 244–255. https://doi.org/10.1016/j.rse.2004.10.006.
Williams, L.E., Araujo, F.J., 2002. Correlations among predawn leaf, midday leaf, and midday stem water potential and their correlations with other measures of soil and plant water status in Vitis vinifera. J. Am. Soc. Hortic. Sci. 127, 448–454.
Wilson, J.W., 1967. The components of leaf water potential. Aust. J. Biol. Sci. 20, 329–348.
Yi, K., Dragoni, D., Phillips, R.P., Roman, D.T., Novick, K.A., 2017. Dynamics of stem water uptake among isohydric and anisohydric species experiencing a severe drought. Tree Physiol. 1–14 .
Zhang, T., Armstrong, R.L., 2001. Soil freeze/thaw cycles over snow-free land detected by passive microwave remote sensing. Geophys. Res. Lett. 28, 763–766. https://doi.org/10.1029/2000GL011952.
Zhou, S., Yu, B., Schwalm, C.R., Ciais, P., Zhang, Y., Fisher, J.B., Michalak, A.M., Wang, W., Poulter, B., Huntzinger, D.N., Niu, S., Mao, J., Jain, A., Ricciuto, D.M., Shi, X., Ito, A., Wei, Y., Huang, Y., Wang, G., 2017. Response of water use efficiency to global environmental change based on output from terrestrial biosphere models. Glob. Biogeochem. Cycles 31. https://doi.org/10.1002/2017GB005733.
Zweifel, R., Item, H., Häsler, R., 2000. Stem radius changes and their relation to stored water in stems of young Norway spruce trees. Trees 15, 50–57. https://doi.org/10.1007/s004680000072.